NANOMATERIALS

Nanocrystals with metastable high-pressure phases under ambient conditions

Tianyuan Xiao¹, Yasutaka Nagaoka¹†, Xirui Wang¹‡, Tian Jiang¹‡, Derek LaMontagne¹, Qiang Zhang¹, Can Cao¹§, Xizheng Diao¹, Jiahua Qiu¹, Yiruo Lu¹, Zhongwu Wang², Y. Charles Cao¹*

The ambient metastability of the rock-salt phase in well-defined model systems comprising nanospheres or nanorods of cadmium selenide, cadmium sulfide, or both was investigated as a function of composition, initial crystal phase, particle structure, shape, surface functionalization, and ordering level of their assemblies. Our experiments show that these nanocrystal systems exhibit ligand-tailorable reversibility in the rock salt—to—zinc blende solid-phase transformation. Interparticle sintering was used to engineer kinetic barriers in the phase transformation to produce ambient-pressure metastable rock-salt structures in a controllable manner. Interconnected nanocrystal networks were identified as an essential structure that hosted metastable high-energy phases at ambient conditions. These findings suggest general rules for transformation-barrier engineering that are useful in the rational design of next-generation materials.

olids from a collection of atoms can adopt a variety of structural phases with their respective physical and chemical properties, providing the foundation for materials discovery (1–3). At ambient temperature and pressure, there is often one thermodynamically stable phase for a given atomic collection, and the rest can potentially become metastable as kinetically trapped phases with positive free energy above the equilibrium state (4). However, a general strategy for engineering kinetic barriers has

yet to be developed but is essential for the rational synthesis of new materials and for expanding the space of synthesizable metastable materials (5, 6).

Phase transformations in bulk solids exhibit complex kinetics involving different microscopic pathways that occur in parallel at different locations within one crystal domain, which are thus difficult to determine experimentally (7). However, transition pressures measured in experiments match well with the theoretical values determined from electronic

structure calculations. For example, the thermodynamic transition in silicon from a diamond to a β -tin structure was calculated to be 8.0 GPa, and this transformation was observed experimentally in the range of 8.8 to 12.5 GPa (8). However, based on elastic stability analysis, Mizushima, Yip, and Kaxiras (MYK) theoretically predicted that defect- and strain-free bulk silicon can remain metastable in the diamond structure up to 64 GPa, which implies a huge intrinsic activation barrier (~0.3 eV per atom) in the structural transformation (9).

This discrepancy indicates that the predicted intrinsic energy barrier in an ideal crystal is drastically decreased by mechanisms associated with defects in real bulk solids during high-pressure experiments and is reflected in high-pressure phases of most bulk solids relaxing back to the ambient phase upon release of pressure. Importantly, the MYK calculation predicts that most high-energy solid phases are theoretically metastable at ambient conditions, if their hosting crystals are defectand strain-free (8, 9). This insight allows for

¹Department of Chemistry, University of Florida, Gainesville, FL 32611, USA. ²Cornell High Energy Synchrotron Source, Cornell University, Ithaca, NY 14853, USA.

*Corresponding author. Email: cao@chem.ufl.edu

†Present address: Department of Chemistry, Brown University, Providence, RI 02912, USA. ‡These authors contributed equally to this work. §Present address: Warren Alpert Medical School of Brown University, Providence, RI 02903, USA.

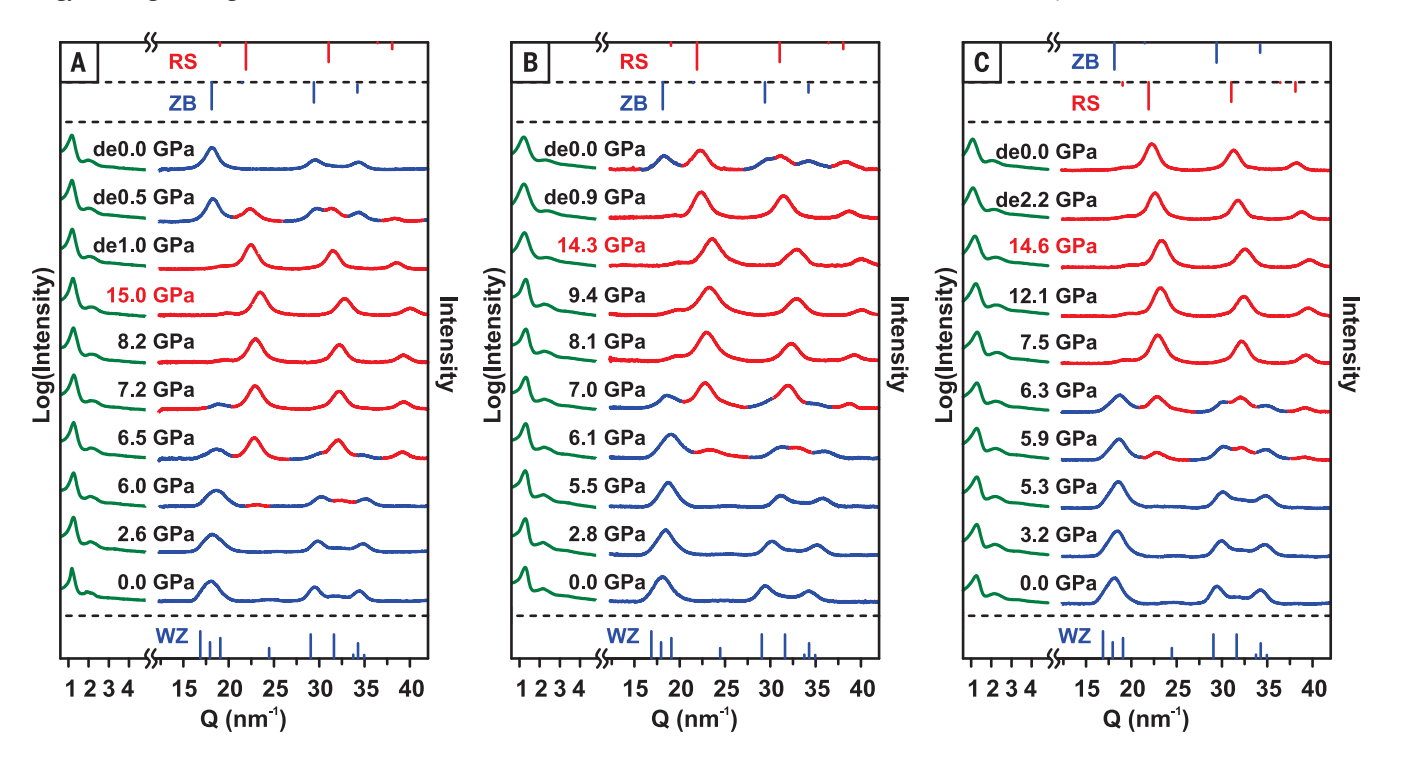


Fig. 1. Ligand-tailorable reversibility of the RS-ZB solid-phase transformation in superlattices of 4.8-nm WZ CdSe nanocrystals. (A to C) WAXS and SAXS patterns collected during compression and decompression (de) at different pressures. CdSe NCs were functionalized with octylamine of (A) 92% surface coverage and of (B) 62% surface coverage and (C) capped with

a mixture of octylamine and CTAB (with a molar ratio of 5:1) of 63% surface coverage in terms of hydrocarbon chains. SAXS patterns are shown in green. WAXS diffraction patterns from the WZ/ZB structure and from the RS structure are shown in blue and red, respectively. See supplementary materials for details on composition-ratio determinations. Q, scattering vector, calculated as $4\pi \sin(2\theta)/\lambda$.

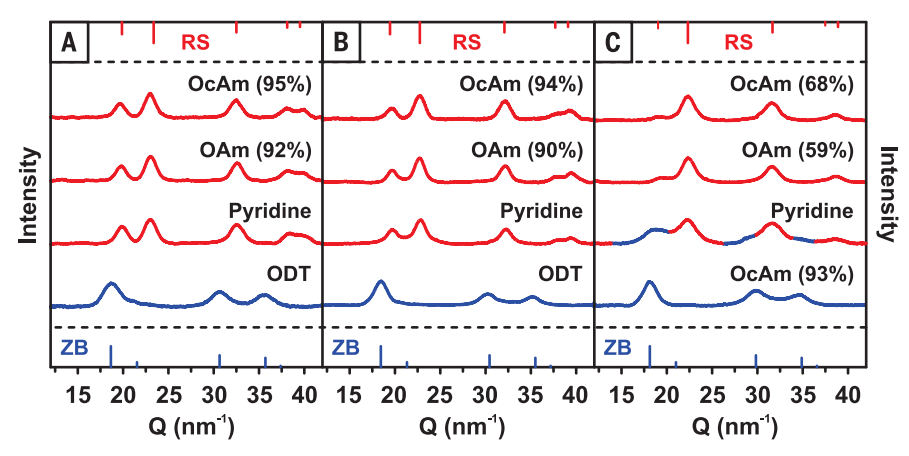


Fig. 2. Ligand-tailorable ambient metastability of the RS phase in 4.8-nm nanospheres. (A to **C**) WAXS patterns of NC assemblies decompressed from a pressure greater than 10.4 GPa: (A) ZB CdS NCs, (B) WZ CdSe/CdS core/shell NCs, and (C) WZ CdS/CdSe core/shell NCs. The type of ligand and surface coverage are given on the corresponding curves for octylamine (OcAm) or oleylamine (OAm). Pyridine ligand is of ~100% surface coverage, and ODT ligand is in excess amount corresponding to ~150% surface coverage. The corresponding WAXS and SAXS patterns obtained at different pressures can be found in figs. S12 to S14 and S16. See supplementary materials for details on ligand composition-ratio determinations.

the development of a general approach for making ambient metastable materials of given chemical compositions based on further understanding of kinetic pathways in solid-solid phase transformations (8).

High-quality colloidal CdSe semiconductor nanocrystals (NCs) (10) have been extensively used as models to study the phase transition from a four-coordinate hexagonal wurtzite (WZ) to a six-coordinate cubic rock-salt (RS) structure (6, 11-16). Bulk CdSe undergoes a WZ-to-RS phase transition at ~2.5 GPa, whereas defect-free WZ CdSe NCs can be metastable at pressures above 6.0 GPa (6, 11), which provides solid evidence for reliability of the MYK calculation (9). Because these NCs can act as single structural domains under high pressures, their phase-transition kinetics are simpler than those of bulk solids and are highly reproducible (12). Such advantages allowed for experimental measurements of fundamental properties-such as the energy, volume, and entropy of activation—of the WZ-to-RS transition in CdSe NCs that revealed directiondependent nucleation through a sliding-plane mechanism (13, 14). However, detailed kinetic pathways for the reverse phase transformation from the six-coordinate RS to the fourcoordinate cubic zinc-blende (ZB) structure remain unclear (14-17).

There exists evidence that under some conditions, high-pressure phases can be retained in NCs upon release of pressure. At ambient conditions, a sample of 11-nm CdSe NCs was composed of ~20% metastable RS structure (15), and a sample of 13-nm PbS nanocubes was composed of 37.2% metastable high-pressure phase (18). Additionally, the RS phase of CdSe/ZnS and CdS NCs could fully persist in a metastable state at ambient pressure (19–23).

These observations suggest the existence of unknown mechanisms for eliminating crystal defects from high-pressure structures (8, 9). To test this hypothesis, we performed a mechanistic study on the reversibility of the RS-ZB transformation in systems comprising spherical NCs or nanorods of CdSe, CdS, or both. We obtained insight into the mechanisms and microscopic processes that determine the kinetic barrier height between two crystal phases.

The ambient metastability of the RS phase in NCs of CdSe, CdS, or both was studied as a function of composition, initial crystal phase, particle structure, shape, surface functionalization, and ordering level of their assemblies. We synthesized six types of spherical NCs with 4.8-nm diameter and one type of CdSe/CdS nanorod with 23.8-nm length and 4.8-nm diameter that exhibited a narrow size distribution and high crystallinity, as confirmed with transmission electron microscopy (TEM), ultraviolet-visible absorption, and fluorescence spectroscopy (figs. S1 to S5). The NC surfaces were precisely controlled through ligand exchange with a designed surface density. We arbitrarily assigned a surface density of five ligands per nm² as 100% ligand coverage. Assemblies of these NCs were prepared either directly on the flat surface of a diamond anvil or at the air-liquid interface of diethylene glycol. To introduce deviatoric stress for promoting interparticle interactions, high-pressure experiments were performed in a diamond anvil cell without the use of a pressure medium (24-27). The solid-state phase structures as a function of pressure were determined with simultaneous measurements of both smallangle and wide-angle x-ray scattering (SAXS and WAXS) at the Cornell High Energy Synchrotron Source.

At ambient conditions, octylamine-capped WZ CdSe NCs (92% coverage; fig. S6A) formed superlattices in a face-centered-cubic (fcc) structure with an interparticle distance of 6.76 nm (Fig. 1A). Upon increasing pressure, the superlattice unit-cell size decreased gradually until 7.2 GPa, above which point the superstructure distorted, whereas the atomic WZ unit-cell volume decreased smoothly up to a threshold pressure (~6.0 GPa), at which point there was an abrupt decrease in unit-cell volume caused by the phase transformation to the RS structure (Fig. 1A). Upon decompression, the distorted fcc superlattice structure recovered in large part, whereas the atomic lattice system completely transformed to a four-coordinate ZB structure (Fig. 1A). Solid-phase transition of the atomic lattice exhibited a hysteresis of ~6.0 GPa, which was close to those measured under a pressure-media environment (6, 14). By contrast, in the sample of CdSe NCs capped with 93% butylamine coverage, a 4.8% RS phase was preserved back to ambient pressure (fig. S7A). These results suggested that ligandshell thickness would play a major role in tailoring the reversibility of the RS-ZB phase transition in CdSe NC systems.

We performed more than 50 synchrotronbased high-pressure experiments to investigate the ambient metastability of RS CdSe structures as functions of amine ligand coverage and alkylchain length, the extent of long-range order in NC assemblies, applied pressure (up to 22 GPa), and decompression rate. At optimized conditions, only 50 to 60% of the RS structures were preserved in decompressed CdSe NC samples (Fig. 1B and fig. S7B). This result indicated that the surface binding of amine ligands may have been too strong and minimized effective interactions between neighboring NCs. However, when pyridine, a weakly binding ligand, was used, the NC assemblies exhibited nearly no long-range order, and no RS structure was retained in the NC system decompressed from 15.0 GPa, whereas after decompression from 16.2 GPa, 3.9% of RS structures were retained (fig. S8). These results suggest that the order of NC assemblies should play a role in the preservation of RS CdSe structures at ambient conditions.

To weaken the average ligand-binding strength while retaining the ability of the NCs to form ordered superstructures, we used a dual-ligand approach with a mixture of a primary amine (as the stronger binding ligand) and cetyltrimethylammonium bromide (CTAB) (as the weaker binding ligand; fig. S6B). The assembly of CdSe NCs functionalized with octylamine and CTAB (5:1 with a coverage of 63%; fig. S6A) formed an fcc superlattice with d₁₁₁-spacing of 5.03 nm (Fig. 1C). The RS-ZB transition became completely irreversible in these assemblies, and the RS CdSe structure was fully preserved at ambient conditions (Fig. 1C). The lattice constant of the fcc superstructure

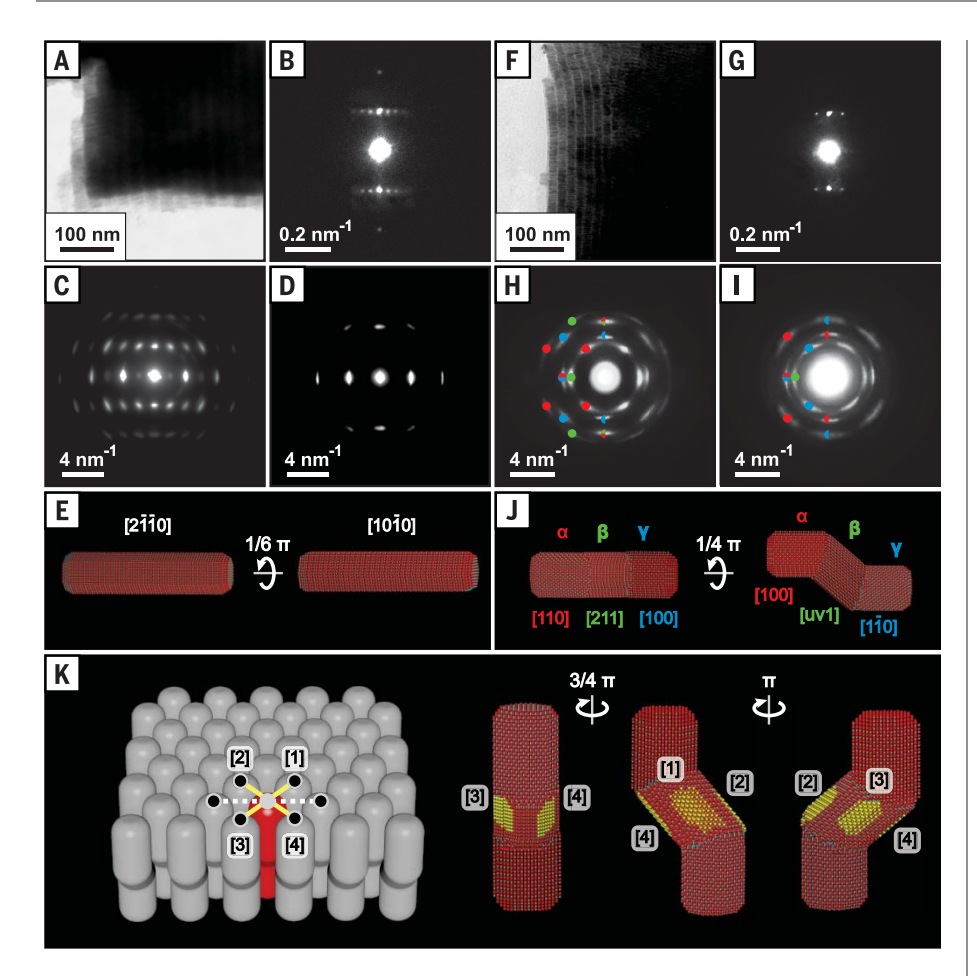


Fig. 3. Superlattice structures of CdSe/CdS WZ nanorods and RS nanorods. (**A** to **D**) Superlattices of WZ nanorods before compression: (A) TEM image, (B) small-angle electron diffraction (SAED) pattern at a 0°-tilt condition, and the wide-angle electron diffraction (WAED) pattern at a (C) 0°-tilt condition with $[2\bar{1}\bar{1}0]$ zone axis and at a (D) 30°-tilt condition with $[10\bar{1}0]$ zone axis. (**E**) 3D atomic nanorod model viewed along the zone axis of corresponding ED patterns shown in (C) and (D), respectively. (**F** to **I**) Superlattices of RS nanorods: (F) TEM image, (G) SAED pattern at a 0°-tilt condition, and the WAED pattern at a (H) 0°-tilt condition and at a (I) 45°-tilt condition, superimposed with simulated diffraction spots from the three corresponding RS domains (see figs. S18 and S19 for details). (**J**) 3D atomic model of a double-bend nanorod with three RS domains (α, β, γ) viewed at angles corresponding to those for ED patterns in (H) and (I), with labeled zone axes, where $u = (\sqrt{3} - 1)$ and $v = (\sqrt{3} - 2)$ at an off-axis direction (see fig. S20 for details). (**K**) Reconstructed 3D superlattice model showing each RS nanorod atomically overlapping with its four neighboring rods at corresponding rectangular areas on their β domains (fig. S22). The RS structures were extremely sensitive to electron beam irradiation and limited our ability to use conventional high-resolution TEM to study detailed features in RS nanostructures (fig. S26).

gradually decreased with a pressure increase up to 7.5 GPa. Above this pressure, the superstructure started to distort (indicated by a continuous expansion of its $d_{\rm HI}$ -spacing) and then irreversibly transformed into a lamellar structure at pressures above ~12.0 GPa (fig. S9). Upon decompression to ambient pressure, the lamellar structure retained its integrity, and its d-spacing further increased to 5.81 nm (Fig. 1C and fig. S9).

Our TEM observations showed that the RS CdSe NCs existed only in the form of aggregates (fig. S10C). After sonication, they could be redispersed into 4.8-nm colloidal particles in

chloroform, but their crystal phase transformed into the ZB structure (fig. S10D). Altogether, these results suggest that strong interparticle associations (such as sintering) may have occurred within the lamellar structures that could be associated with the ambient metastability of the RS CdSe structure. Similar ligand-tailorable phenomena were observed in CdSe NCs capped with butylamine and CTAB ligands (fig. S7C).

The formation energy of ZB CdSe is 1.0 meV per atom lower than that of the WZ form, and such NCs were enclosed by crystal facets different from those of WZ (28). However, no substantial differences were observed between

4.8-nm ZB and WZ CdSe NCs in both the pressure-induced transformation to the RS structure and the ligand-tailorable reversibility of the RS-ZB phase transitions (fig. S11). Pure ambient metastable RS CdSe NCs can also be synthesized from ZB NCs (fig. S11B), showing that the initial crystal phase was not important for the ambient metastability of the resulting RS structures, and RS NCs that were transformed from the ZB and WZ phases could have degenerate three-dimensional (3D) atomic fine structures (29).

Bulk CdS, like CdSe, undergoes a reversible solid-phase transformation from a four- to sixcoordinate structure at a pressure of ~2.5 GPa (30). However, CdS NCs exhibited substantial differences in the ligand-tailorable reversibility of their RS-ZB phase transition when compared with their CdSe counterparts (Fig. 2A). Dualligand functionalization was not necessary for making ambient metastable RS CdS NCs. Upon decompression from a pressure above 10.4 GPa, the RS phase was fully preserved in assemblies made from 4.8-nm ZB CdS NCs capped with amine ligand coverage as high as 95%, or even capped with 100% pyridine ligands, in which case NC assemblies exhibited no long-range order (Fig. 2A and fig. S12, A to C). By contrast, in assemblies of CdS NCs functionalized with excess octadecanethiol (ODT) (a stronger binding ligand than amines, for isolating CdS NCs as separate particles at high pressures), the RS-ZB phase transformation was completely reversible even when decompressed from 15.2 GPa (Fig. 2A and fig. S12D). These results demonstrated that the RS CdS phase was not intrinsically metastable at the nanometer scale, suggesting that the observed metastability in CdS NCs should also be related to strong interparticle associations, as in the case of RS CdSe NCs.

To further explore effects induced by chemical composition and particle structure, we synthesized 4.8-nm CdSe/CdS core/shell NCs in a WZ or ZB structure from corresponding 3.4-nm CdSe cores, and 4.8-nm WZ CdS/CdSe core/shell NCs from 3.4-nm CdS cores (figs. S3 and S4). In terms of the ligand-tailorable reversibility of the RS-ZB phase transition, both WZ and ZB CdSe/CdS NCs exhibited a nearly identical property to CdS NCs (Fig. 2B and figs. S13 to S15), whereas the behavior of CdS/CdSe NCs was in between that of CdS and CdSe NCs (Fig. 2C and fig. S16). Together, these results demonstrate that the composition of shell and core both play important roles in maintaining the RS phase at ambient conditions.

To study NC shape effects, we prepared atomically aligned nanorod superlattices at an air-liquid interface using 23.8-nm WZ CdSe/CdS nanorods functionalized with 95% octylamine coverage. These superlattices could be indexed as a simple hexagonal structure with lattice parameters of a=6.72 nm and c=26.2 nm, where the atomic WZ lattice of the CdSe/CdS

nanorods was coaxially aligned with the superlattice (fig. S17, A to C, and Fig. 3, A to E). After the pressure increase to 6.3 GPa, CdSe/CdS nanorods exhibited a WZ-RS phase transition at a pressure range slightly lower than that of the 4.8-nm CdSe/CdS core/shell nanospheres.

When decompressed from a pressure greater than ~10.0 GPa, the RS phase was fully preserved at ambient conditions (fig. S17A). During this process, the hexagonal superlattice structure was largely retained but was accompanied by a substantial d-spacing decrease in the c-axis direction, adopting a new set of lattice parameters of a = 6.97 nm and c = 17.5 nm (Fig. 3, F and G, and fig. S17A). As indicated by the dotlike electron diffraction (ED) patterns, the threedimensionally ordered atomic alignments of CdSe/CdS nanorods persisted in the RS phase in the superlattices (Fig. 3, H and I). Altogether, our experimental data suggest that in this process, WZ CdSe/CdS nanorods transformed into double-bend RS nanorods with three domains, exhibiting a height of ~15.8 nm and an angle of 125.3° between neighboring domains (Fig. 3, F to J, and figs. S18 to S20). This shape change involved a shearing motion of the (0001) WZ crystal planes, which is consistent with the direction-dependent nucleation model of the WZ-to-RS transition proposed by Alivisatos and co-workers (12, 14, 16).

The formation of three-domain nanorods is also consistent with TEM observations of the ZB nanorods recovered from RS aggregates (fig. S10, K and L). The recovered nanorods, having sizes similar to those of the nanorods before compression, exhibited traces of shape deformation and contained multiple crystalline domains and curved lattice fringes caused by strain (fig. S21). Based on all of the structural data, a reconstructed superlattice model showed that each double-bend nanorod atomically overlapped with four neighbors at the corresponding rectangular areas on the surfaces of their β domains, suggesting the existence of interparticle sintering, which would be responsible for the metastability of the RS phase (Fig. 3K and fig. S22). Indeed, in the assemblies of CdSe/ CdS nanorods functionalized with excess strongbinding ODT ligands, the RS-ZB phase transition became fully reversible, and no detectable RS phase was observed when decompressed even from 12.5 GPa (figs. S10J and S17D).

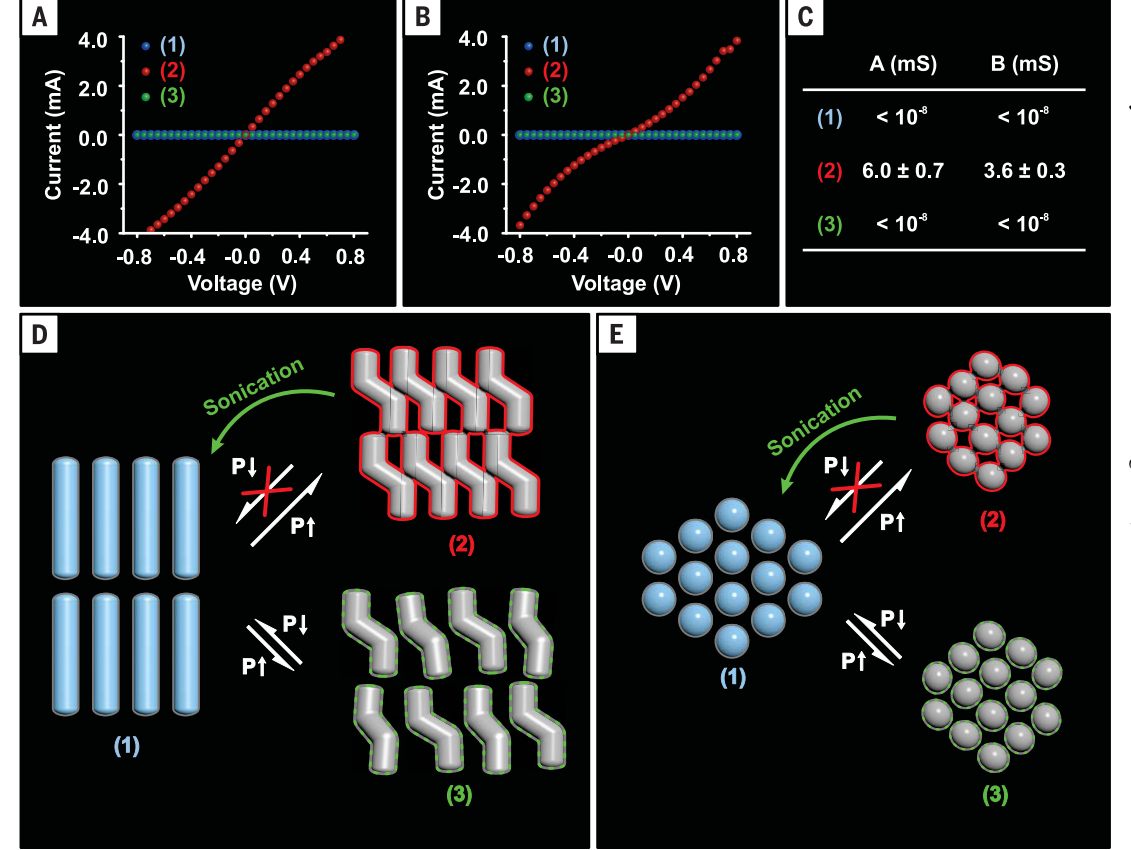
Additional information regarding interparticle sintering was obtained from electrical conductivity measurements (31). Films, composed of either WZ structures recovered before

the WZ-RS transition or ZB structures that transformed from the RS phase, were insulating below the detection limit (<10 pS), whereas the films of RS structures exhibited conductivities at least eight orders of magnitude higher, ranging from 3.0 to 8.0 mS (Fig. 4, A to C). These results, together with TEM observations, provide evidence that the ambient metastable RS phase existed in the form of three-dimensionally interconnected and partially fused NC networks created by interparticle sintering (Figs. 3 and 4 and fig. S10). These findings also suggest that the observed ligand-tailorable reversibility of their RS-ZB phase transition was caused by ligand effects during interparticle sintering, in which surface-ligand rearrangement was the initial step for the surface-atom diffusion and chemical-bond formation (32).

Based on these results, we propose that interparticle sintering was a main process that eliminated crystal defects and relaxed lattice distortions from high-pressure RS structures. The partial restoration of the intrinsic kinetic barrier in ideal crystals (as predicted by MYK) created ambient metastable nanostructures (Fig. 4, D and E). The RS NCs that formed from pressure-induced solid-phase transitions comprised a large quantity of high-energy crystal

Fig. 4. Electrical conductivity as indictor of interparticle sintering. (A and B) The current-voltage curve for films composed of assemblies of (A) 23.8-nm WZ CdSe/CdS nanorods and (B) 4.8-nm WZ CdSe/CdS core/shell nanospheres in (1) the WZ phase before phase transition obtained by decompression from ~1.8 GPa, (2) the ambient stable RS phase obtained by decompression from ~10.4 GPa, or (3) the ZB phase that transformed from RS NCs with excess ODT after decompression from ~12.5 GPa. (**C**) Measured conductivity is shown in column A for nanorods and column B for nanospheres. (D and E) Schematic of proposed interparticle sintering mechanism for nanorods and nanospheres, respectively: (1) initial nanostructures at ambient pressure, (2) the RS phase in the form of interconnected NC networks at a high pressure (fig. S10, C, G, and K), and

(3) the RS phase in the form of



"free" NCs isolated with strong-binding ligands at high pressures. In recovered samples after decompression, either no or low degrees of interparticle sintering were observed with TEM (fig. S10, B, F, and J). P, pressure.

defects and lattice distortions (12) and served as nucleation sites for the rapid RS-to-ZB and RS-to-WZ transitions observed in the systems with no or low degrees of interparticle sintering (fig. S10, B, F, and J) (6, 11-14). In high-pressureand/or deviatoric-stress-induced interparticle sintering, solid-state chemical reactions—driven by the minimization of Gibbs free energy-take place between surface atoms, forming effective sinks to absorb local high-energy defects and lattice distortions (33). These reactions produce grain and/or twin boundaries (GTBs) between neighboring particles (fig. S23, A and B) to form three-dimensionally interconnected nanocrystal networks in which crystal defects can be delocalized through stress-driven diffusion or propagation (34). This process allowed delocalized and collective GTB-defect interactions within an interconnected network where GTBs act as sources, sinks, or both to eliminate crystal defects through absorption and annihilation (note that GTBs also occurred within a single double-bend nanorod; fig. S23B) (35, 36).

Moreover, GTBs further acted as obstacles to block or jam dislocation motions and stabilize and harden interconnected NC networks (37, 38) and provided additional mechanisms to raise the activation barrier height for the RS-to-ZB transformation (fig. S23, C and D). These defect-elimination and strain-relaxation mechanisms depended on the hydrostatic and deviatoric stress applied on the system (24, 25). Our experimental findings showed that the activation barrier height in resulting RS structures was strongly dependent on the highest applied pressure, indicated by the observed partial reversibility of the RS-ZB transition in samples decompressed from lower pressures (figs. S13, S17, and S24). These results further demonstrate a critical pressure for a given NC system, above which point the resulting interconnected NC networks can fully retain the RS phase at ambient conditions (fig. S24).

This interparticle sintering (or partial fusion) mechanism is in good agreement with the entire set of experimental observations as well as the MYK prediction (8, 9). Without pressure media, the formation of three-dimensionally interconnected NC networks strongly interplays with an emergent phenomenon called force chain networks (39), which are created by interparticle interactions and by the topological patterns of pressure applied within the system (39, 40). Thus, the order of NC assemblies affects the degree of interparticle sintering as well as the mechanical integrity and strain uniformity of the resulting interconnected networks (Figs. 1C and 2C and fig. S8). In disordered systems, NC shape anisotropy promotes the formation of anisotropic force-chain-network architectures (40, 41), yielding strained-NC networks and thus imposing additional effects

on the ambient metastability of high-pressure phases. Indeed, when the ordering level of hexagonal-superlattice structures was decreased, CdSe/CdS nanorod assemblies retained 77.8% of the RS phase, whereas 100% was still preserved in totally disordered assemblies of CdSe/CdS nanospheres (figs. S14A and S25). In addition, the observed composition dependence in the ligand-tailorable reversibility of the RS-ZB phase transition likely originated from differences in the chemical and mechanical properties regarding interparticle sintering, as well as the formation, elimination, propagation, and annihilation of crystal defects and the relaxation of lattice distortions in the interconnected NC systems (29, 32-41).

To date, metastable RS CdSe, CdS, and CdSe/CdS samples in our lab have been fully preserved under ambient conditions for more than 6 years. This extended lifetime shows that an apparent activation-energy barrier of more than 1.3 eV per particle was created in the RS-to-ZB solid phase transformation (8, 20). The strategy for engineering transformation barriers established in this work is readily generalizable for making ambient metastable high-energy phases of other materials such as IV-VI and III-V semiconductors and transitionmetal chalcogenides. In addition, our findings identify interconnected nanocrystal networks as a new form of matter that can effectively host metastable high-energy phases at ambient conditions. This approach allows for the rational design of synthetic methods for metastable materials through low-pressure routes (42), opening new opportunities for materials discovery and fabrication (2-5).

REFERENCES AND NOTES

- W. F. Smith, Principles of Materials Science and Engineering (McGraw-Hill, ed. 3, 1996).
- 2. W. Sun et al., Sci. Adv. 2, e1600225 (2016)
- 3. H. Koinuma, I. Takeuchi, Nat. Mater. 3, 429-438 (2004).
- A. Parija, G. R. Waetzig, J. L. Andrews, S. Banerjee, J. Phys. Chem. C 122, 25709–25728 (2018).
- M. Aykol, S. S. Dwaraknath, W. Sun, K. A. Persson, *Sci. Adv.* 4, eaaq0148 (2018).
- C. C. Chen, A. B. Herhold, C. S. Johnson, A. P. Alivisatos, Science 276, 398–401 (1997).
- 7. J. M. Besson et al., Phys. Rev. B 44, 4214-4234 (1991).
- L. E. Brus, J. A. W. Harkless, F. H. Stillinger, J. Am. Chem. Soc. 118, 4834–4838 (1996).
- K. Mizushima, S. Yip, E. Kaxiras, Phys. Rev. B 50, 14952–14959 (1994).
- C. B. Murray, D. J. Norris, M. G. Bawendi, J. Am. Chem. Soc. 115, 8706–8715 (1993).
- S. H. Tolbert, A. P. Alivisatos, Science 265, 373–376 (1994).
- J. N. Wickham, A. B. Herhold, A. P. Alivisatos, *Phys. Rev. Lett.* 84, 923–926 (2000).
- K. Jacobs, A. P. Alivisatos, Rev. Mineral. Geochem. 44, 59–72 (2001).
- K. Jacobs, D. Zaziski, E. C. Scher, A. B. Herhold,
 A. Paul Alivisatos, *Science* 293, 1803–1806 (2001).
 K. Jacobs, J. Wickham, A. P. Alivisatos, *J. Phys. Chem. B* 106,
- 3759–3762 (2002). 16. D. Zaziski et al., Nano Lett. **4**, 943–946 (2004).
- D. Zaziski et al., Nano Lett. 4, 943–946 (2004).
 M. Grünwald, E. Rabani, C. Dellago, Phys. Rev. Lett. 96, 255701 (2006).
- 18. T. Wang et al., Adv. Mater. 27, 4544-4549 (2015)
- 19. Z. Li et al., Phys. Status Solidi B 248, 1149-1153 (2011).

- M. Grünwald, K. Lutker, A. P. Alivisatos, E. Rabani, P. L. Geissler, Nano Lett. 13, 1367–1372 (2013).
- 21. R. Martín-Rodríguez et al., J. Appl. Phys. **111**, 063516 (2012).
- H. Zhu et al., J. Am. Chem. Soc. 139, 8408–8411 (2017).
- 23. L. Meng et al., J. Am. Chem. Soc. **142**, 6505–6510 (2020).
- 24. W. Li, H. Fan, J. Li, Nano Lett. 14, 4951–4958 (2014).
- 25. B. Li et al., Sci. Adv. 3, e1602916 (2017).
- K. Bian, A. K. Singh, R. G. Hennig, Z. Wang, T. Hanrath, Nano Lett. 14, 4763–4766 (2014).
- 27. P. Podsiadlo et al., Nano Lett. 11, 579-588 (2011).
- The Materials Project, Materials Project database; https://materialsproject.org.
- 29. B. H. Kim et al., Science 368, 60-67 (2020).
- 30. H. Sowa, Solid State Sci. 7, 73-78 (2005).
- 31. D. Yu, C. Wang, P. Guyot-Sionnest, *Science* **300**, 1277–1280 (2003).
- 32. L. Wang et al., Science 337, 825-828 (2012).
- S. Tanaka, in *Materials Chemistry of Ceramics*, J. Hojo, Ed. (Springer, 2019).
- 34. P. Heitjans, J. Karger, Eds., Diffusion in Condensed Matter: Methods, Materials, Models (Birkhauser, ed. 2, 2005).
- X. M. Bai, A. F. Voter, R. G. Hoagland, M. Nastasi,
 B. P. Uberuaga, *Science* 327, 1631–1634 (2010).
- J. Beyerlein, M. J. Demkowicz, A. Misra, B. P. Uberuaga Prog. Mater. Sci. 74, 125–210 (2015).
- 37. K. Lu, *Nat. Rev. Mater.* **1**, 16019 (2016).
- 38. X. Zhou, X. Y. Li, K. Lu, Science **360**, 526–530 (2018).
- S. Ostojic, E. Somfai, B. Nienhuis, *Nature* **439**, 828–830 (2006).
- K. P. Krishnaraj, P. R. Nott, *Phys. Rev. Lett.* **124**, 198002 (2020).
- 41. E. Azéma, F. Radjaï, Phys. Rev. E 85, 031303 (2012).
- 42. P. F. McMillan, Nat. Mater. 1, 19-25 (2002).

ACKNOWLEDGMENTS

T.J. and X.W. contributed equally to this work. We thank the Research Service Centers (RSC) at the University of Florida for TEM usage. We thank B. Gao for the use of a thermogravimetric analyzer. We thank F. So in the Department of Materials Science and Engineering at the North Carolina State University for electric conductivity measurements. Funding: This work was supported by the National Science Foundation (DMR1710509, DMR1309798, DMR-1332208, and DMR-1829070) and special funds from the College of Liberal Arts and Science of the University of Florida. Author contributions: Y.C.C., T.X., and Y.N. conceived and designed experiments. T.X., T.J., X.W., C.C., and Y.N. performed the experiments and analyzed data. D.L., Y.L., J.O., and O.Z. participated in the early stages of the project. synthesized nanocrystals, and participated in data analysis. T.X., T.J., Y.N., J.Q., Q.Z., and X.D. designed, performed beamline synchrotron studies. T.X. and Y.N. performed TEM measurements and data simulations. Z.W. initiated this project, designed beamline synchrotron studies, and analyzed data. Y.C.C. supervised the entire project, analyzed data, and participated in simulations. Y.C.C., Z.W., and T.X. co-wrote the paper. All authors discussed the results and commented on the manuscript. Competing interests: The authors declare that they have no

competing interests. **Data and materials availability:** All data needed to evaluate the conclusions in the paper are present in the main text or the supplementary materials. The samples can be provided by the authors upon reasonable request under a materials transfer agreement with the University of Florida. Requests for materials should be addressed to the corresponding author. **License information:** Copyright © 2022 the authors, some rights reserved; exclusive licensee American Association for the Advancement of Science. No claim to original US government works. https://www.science.org/about/science-licenses-journal-article-reuse

SUPPLEMENTARY MATERIALS

science.org/doi/10.1126/science.abq7684 Materials and Methods Supplementary Text Figs. S1 to S30 Table S1 References (43–50)

Submitted 29 April 2022; accepted 30 June 2022 10.1126/science.abg7684



Nanocrystals with metastable high-pressure phases under ambient conditions

Tianyuan XiaoYasutaka NagaokaXirui WangTian JiangDerek LaMontagneQiang ZhangCan CaoXizheng DiaoJiahua QiuYiruo LuZhongwu WangY. Charles Cao

Science, 377 (6608), • DOI: 10.1126/science.abq7684

Ligand-driven metastability

A high-pressure phase of a solid can persist at ambient pressure if there are kinetic barriers to its relaxation. Xiao *et al.* performed detailed mechanistic studies on the reversibility of four- to six-coordinate pressure-driven solid-phase transitions in well-controlled model systems of nanospheres or nanorods of cadmium selenide, cadmium sulfide, or both (see the Perspective by Mao and Lin). The choice of surface ligands could control the reversibility of the transformations. Interparticle sintering helped to eliminate crystal defects and relaxed lattice distortions from the high-pressure rock-salt structures to maintain their ambient-pressure metastability. —PDS

View the article online

https://www.science.org/doi/10.1126/science.abq7684

Permissions

https://www.science.org/help/reprints-and-permissions

Use of this article is subject to the Terms of service